Dual Model Equivalent Inductance Method for Identifying Transformer Inrush Current

Jimin Chai, Yuping Zheng, and Shuyan Pan

***Abstract*—Based on the dual equivalent model of a single-phase two-winding transformer and a single-phase three-winding autotransformer, a method for identifying inrush current in single-phase transformers is proposed. This method distinguishes inrush current from internal fault current using the instantaneous equivalent inductance of the dual model. The setting principle of the method is determined by analyzing the air-core inductance and the equivalent model of the faulty transformer. PSCAD simulations and recorded transformer protection data demonstrate that the proposed method can accurately identify inrush current when the transformer core is deeply saturated, and can quickly discriminate between currents during a critical internal fault. Furthermore, the simulation results show that the proposed method is sensitive to minor turn-to-turn faults but is less sensitive to the equivalent impedance of an external source.**

***Index Terms*—Air-core inductance, differential current, dual equivalent model, equivalent inductance, inrush current, internal fault.**

I. Introduction

In power systems, the differential protection method safeguards power transformers during internal faults. However, when a transformer is energized, the inrush current may cause differential protection malfunction. As a result, distinguishing inrush current from internal fault current is important for transformer protection.

Currently, the discrimination methods are classified as follows.

1) Harmonic restraint methods [1], [2]. These methods rely on harmonic current, particularly the second-harmonic current. They are widely used due to their simplicity. However, the harmonics in the inrush current may be low because of the high magnetic permeability of modern transformer core materials, reducing discrimination accuracy.

2) Pattern recognition methods [3]–[5]. These methods differentiate inrush and internal fault currents based on their waveform characteristics, such as symmetry and dead angle. However, they do not account for the physical core saturation mechanism and introduce difficulties in setting parameters for transformer protection.

3) Artificial intelligence methods [6]–[9]. These methods employ artificial intelligence and machine learning to identify inrush current waveforms. However, they require large amount of training data, and their algorithms are complex.

4) Power differential methods [10], [11]. These methods employ differential power to distinguish inrush current from internal fault current. However, the data windows in the algorithms are wide, and setting parameters for power loss is challenging.

5) Frequency analysis methods [12]–[15]. These methods utilize wavelet transform of the current in the time and frequency domains. However, they require wide data windows and are susceptible to noise.

6) Flux-restrained and equivalent model-based methods [16]–[19]. These methods rely on the equivalent operation model of transformers. They use equivalent parameters (e.g., flux, inductance, or admittance) to discriminate inrush current from internal fault current. They can determine when the transformer core alternates between saturated and unsaturated states during the transient period of inrush current. However, they lack clear setting principles, and certain parameters must be determined through field experiments, limiting their effectiveness in protecting transformers.

Currently, the most widely used methods for identifying inrush current still rely on the second harmonic content. However, decrease in the saturation knee point of new ferromagnetic materials increases the likelihood of deep saturation of the transformer core, thereby reducing the second harmonic content of the inrush current. Moreover, the increasing number of grid connec-

Received: August 30, 2024
Accepted: March 1, 2025
Published Online: July 1, 2025

Jimin Chai (corresponding author) is with the School of Electrical and Information Engineering, Changzhou Institute of Technology, Changzhou 213032, China; and the School of Electrical and Power Engineering, Hohai University, Nanjing 211100, China (e-mail: chaijm@czu.cn).

Yuping Zheng is with NARI Group Corporation (State Grid Electric Power Research Institute), Nanjing 211106, China; and the School of Electrical and Power Engineering, Hohai University, Nanjing 211100, China (e-mail: zhengyuping@sgepri.sgcc.com.cn).

Shuyan Pan is with NARI Group Corporation (State Grid Electric Power Research Institute), Nanjing 211106, China (e-mail: panshuyan@sgepri.sgcc.com.cn).

DOI: 10.23919/PCMP.2024.000128

tions for photovoltaic, wind, and other new power generation systems may increase the equivalent impedance of the external system of a given transformer. Consequently, the fault current may decrease during an internal fault, potentially affecting the speed and sensitivity of internal fault identification. Therefore, developing an improved method for identifying inrush current that is suitable for these modified saturation and fault conditions is crucial.

In this paper, a novel method for discriminating the inrush currents of single-phase transformers based on the instantaneous equivalent inductance of the dual model is proposed. PSCAD simulations and tests of recorded transformer protection data show that this method can accurately identify inrush current even when the transformer core is deeply saturated. Furthermore, the method can quickly identify critical internal faults, regardless of the equivalent impedance of the external system.

The remainder of this paper is structured as follows. In Section II, the equivalent model is analyzed based on the duality principle of a single-phase two-winding transformer and the equivalent model of a faulty transformer, and a unified model of equivalent inductance is then proposed. Section III analyzes the algorithm of the equivalent inductance and designs the discrimination scheme and its setting principle accordingly. In Section IV, the proposed method is applied to a single-phase three-winding autotransformer, whereas Section V verifies the efficacy of the proposed method using PSCAD simulations and recorded transformer protection data. Finally, Section VI presents the conclusions of the study.

II. Theory of Equivalent Model

A. Dual Equivalent Model

Methods based on the transformer equivalent model can reflect the real-time operating status of the transformer core. For example, during the transient period of inrush current, the core repeatedly alternates between saturated and unsaturated states. Studies on single-phase two-winding transformers often use the T model [17], [19] and Γ model [20], although most studies on transformers are based on the T model derived from the operation equation of a two-winding transformer. The T model is simple and has been widely used in studies on inrush current. Nevertheless, it has two shortcomings. First, the sum of the leakage inductances of the primary and secondary windings is obtained via the transformer short circuit test, but the individual leakage inductances cannot be obtained. Second, the results produced by the T model and those obtained by actual measurements may differ, especially when the transformer core is deeply saturated [20]–[25]. The Γ equivalent model places the equivalent magnetizing branch on one winding of the transformer, so if the external power source is on another winding, the calculation error is significant [20]. Compared to the T and Γ equivalent models, the dual equivalent model [20]–[25], which is based on magnetic circuit and circuit duality theory, more accurately reflects the magnetic flux distribution of transformers and achieves higher computational accuracy, particularly when the transformer core is deeply saturated. Therefore, designing a new inrush current identification method based on a more accurate dual model is of great significance for transformer protection.

Figure 1 shows a dual equivalent model called the Π model, which consists of two shunt magnetizing branches and one leakage inductance branch. Compared to the T model, the Π model, which is based on the principle of duality between magnetic and electric circuits, produces more accurate calculations [20]–[25]. Furthermore, the leakage inductance L_{12} can be determined using the short circuit test parameters listed on the transformer nameplate. Therefore, the Π model can enable new inrush current identification criteria to be designed according to the leakage inductance L_{12}.

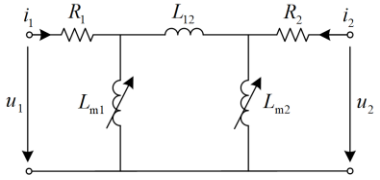

Fig. 1. Π equivalent model of single-phase two-winding transformer.

In Fig. 1, the nonlinear inductances L_{m1} and L_{m2} represent the equivalent inductances of the magnetic circuits m_1 and m_2, respectively, as shown in Fig. 2; the linear inductance L_{12} represents the equivalent leakage inductance of the magnetic circuit m_{12}, which is also shown in Fig. 2; furthermore, u_1 and u_2 denote the voltages of the primary and secondary windings, respectively; while i_1 and i_2 denote the currents in the primary and secondary windings, respectively.

Figure 2 shows the layout of the core (with radius r) and windings of a single-phase two-winding transformer. In Fig. 2, m_1, m_2, and m_{12} represent the magnetic circuits corresponding to the side limb, core, and leakage magnetic flux, respectively; windings 1 and 2 are the outer (primary) and inner (secondary) windings with thicknesses a_1 and a_2, respectively; the two windings are separated by the distance d_{12}; and h_{eq} is the equivalent height of the windings.

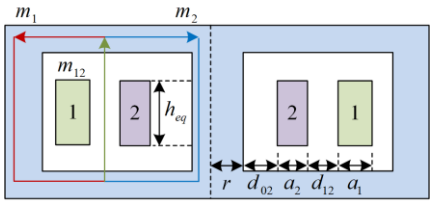

Fig. 2. Layout of single-phase two-winding transformer.

B. Equivalent Model for Calculation

Although the delta-wye transformation cannot be directly applied to nonlinear elements, it can still be used for transformer flux and piecewise linearization, as explained in [26]. The Π model, which has a delta structure (as shown in Fig. 1 or Fig. 3(a)), can be transformed into a model with a wye structure, as shown in Fig. 3(b).

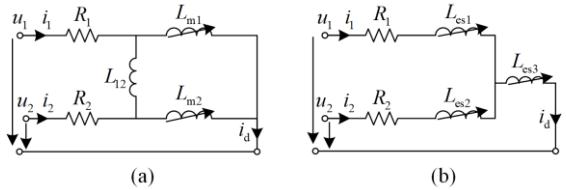

Fig. 3. Equivalent inductance model. (a) Model with delta structure. (b) Model with wye structure.

The differential current i_d of the two windings (shown in Fig. 3(a)) is calculated as:

$$i_d = i_2 + i_1 \tag{1}$$

The values of L_{es1}, L_{es2}, and L_{es3} (shown in Fig. 3(b)) are calculated as follows:

$$L_{es1} = \frac{L_{m1}L_{12}}{L_{12} + L_{m1} + L_{m2}} \tag{2}$$

$$L_{es2} = \frac{L_{12}L_{m2}}{L_{12} + L_{m1} + L_{m2}} \tag{3}$$

$$L_{es3} = \frac{L_{m1}L_{m2}}{L_{12} + L_{m1} + L_{m2}} \tag{4}$$

When the inrush current flows, the core is unsaturated for $t \in (t_1, t_2)$ and saturated for $t \in (t_2, t_3)$, as shown in Fig. 4.

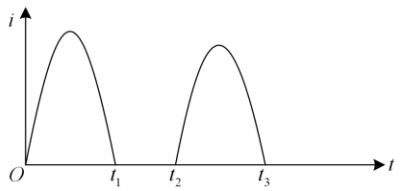

Fig. 4. Waveform of transformer inrush current.

The process of energizing from winding 1 (for instance) can be analyzed in two cases.

Case 1: If the core is unsaturated, the magnetizing current is extremely small, so u_1 and u_2 are approximately equal when one winding voltage is converted to another via the transformer ratio. Thus, u_1 and u_2 can be connected in parallel to generate an additional equivalent circuit, as shown in Fig. 5.

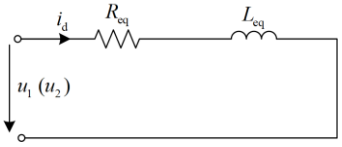

Fig. 5. Equivalent inductance model for Case 1.

According to Fig. 3(b) and Fig. 5, if the resistance is ignored and the core is unsaturated, L_{eq} can be calculated as:

$$L_{eq} \approx L_{es1} // L_{es2} + L_{es3} = L_{m1} // L_{m2} \tag{5}$$

Since L_{m1} and L_{m2} represent the magnetizing inductances of the core and L_{12} represents the leakage flux, L_{eq} can be significantly larger than L_{12} when the transformer core is unsaturated, even by several orders of magnitude.

Case 2: If the core is saturated, the voltages on both sides of the transformer will not be equal due to the voltage drop caused by the large magnetizing current, particularly under deep saturation. Assuming that the transformer is energized from winding 1, u_1 will be greater than u_2 because of the voltage drop, and thus, u_1 and u_2 shown in Fig. 3(b) cannot be connected in parallel. Therefore, when the core is saturated, the equivalent circuit in Fig. 5 is invalid. In this case, a virtual inductor ΔL_{es2}, which is proportional to L_{es2} shown in Fig. 3(b), is added to obtain a virtual voltage u_{2e}, where $u_{2e} \approx u_1$, as shown in Fig. 6(a). Using the original model in Fig. 6(a), the transformed model in Fig. 6(b) and the final equivalent model in Fig. 6(c) can be obtained.

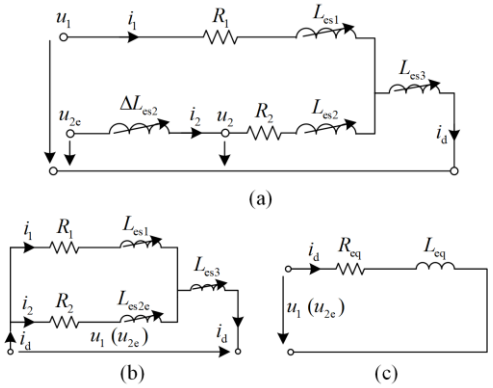

Fig. 6. Equivalent inductance model for Case 2. (a) Original model. (b) Transformed model. (c) Final equivalent model.

In Fig. 6(a), because ΔL_{es2} is proportional to L_{es2}, L_{es2e} can be calculated as:

$$L_{es2e} = k_{es2e} L_{es2} \tag{6}$$

where $k_{es2e} > 1$. According to Figs. 6(b) and (c), if the core is saturated, then L_{eq} can be calculated via:

$$L_{eq} \approx L_{es1} // L_{es2e} + L_{es3} = (L_{es1} L_{es2e}) / (L_{es1} + L_{es2e}) + L_{es3} \tag{7}$$

According to (2), L_{es1} is less than L_{12}, so $L_{es1} // L_{es2e}$ is less than L_{12}. According to (4), L_{es3} is less than $L_{m1} // L_{m2}$, and thus, L_{eq} in (7) is less than $L_{m1} // L_{m2} + L_{12}$. The values of L_{m1} and L_{m2} for the deeply saturated core are significantly smaller than those for the unsaturated core. In addition, the value of L_{eq} in (7) is smaller than in (5) when the core is unsaturated.

According to (6) and (7), because $k_{es2e} > 1$ and $L_{es2e} > L_{es2}$, the value of L_{eq} in (7) is greater than $L_{es1} // L_{es2} + L_{es3}$. Thus, L_{eq} is greater than the corresponding value of $L_{m1} // L_{m2}$ when the core is saturated.

For field transformers, the voltage transformers are generally installed on the busbars. When energizing from winding 1 (for instance), only u_1 can be measured, but u_2 cannot. According to the analysis of both cases shown in Figs. 5 and 6, when energizing from winding 1, the unified calculation model based on u_1 and i_d can be represented by the diagram shown in Fig. 7, regardless whether the core is saturated or not.

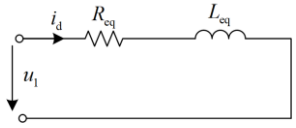

Fig. 7. Unified equivalent inductance model.

According to an analysis based on (5), the value of L_{eq} is extremely large relative to L_{12} when the core is unsaturated. Conversely, an analysis based on (7) shows that L_{eq} is small when the core is deeply saturated.

C. Air-core Inductance

The concept of air-core inductance is analyzed in detail in [21] and [22]. Assuming that the core is fully saturated and its permeability is the same as that of a vacuum, the equivalent inductance obtained from the port of the dual equivalent circuit is the air-core inductance.

As shown in Fig. 1, if $i_2 = 0$ and the core is fully saturated, u_1 and i_1 can be used to calculate the air-core inductance of winding 1. By ignoring the resistance, as presented in [24], the air-core inductance of winding 1 can be calculated as:

$$L_{air\text{-}out} = \frac{L_{m1-sat}(L_{12} + L_{m2-sat})}{L_{12} + L_{m2-sat} + L_{m1-sat}} \tag{8}$$

where L_{m1-sat} and L_{m2-sat} are equal to the values of L_{m1} and L_{m2}, respectively, when the core is fully saturated. Similarly, the air-core inductance of winding 2 can be calculated using:

$$L_{air\text{-}in} = \frac{L_{m2-sat}(L_{12} + L_{m1-sat})}{L_{12} + L_{m2-sat} + L_{m1-sat}} \tag{9}$$

The air-core inductance can be analyzed according to the layout of the inner and outer windings. We assume that only winding 1 is connected to an external source for excitation. If the core is fully saturated and its permeability is equal to that of a vacuum, then winding 1 is an equivalent air-core coil and the air-core inductance can be calculated as:

$$L_{air\text{-}out} = \left(\mu_0 N^2 \pi r_{eq1}^2\right) / h_{eq} = \left(\mu_0 N^2 \pi A_{eq1}\right) / h_{eq} \tag{10}$$

where $L_{air\text{-}out}$ is the air-core inductance of the series winding; $r_{eq1} = r + d_{02} + a_2 + d_{12} + 0.5a_1$; $A_{eq1} = r_{eq1}^2$; N is the equivalent number of windings; and μ_0 is the permeability of the vacuum. In addition, $L_{air\text{-}in}$ can be calculated as:

$$L_{air\text{-}in} = \left(\mu_0 N^2 \pi r_{eq2}^2\right) / h_{eq} = \left(\mu_0 N^2 \pi A_{eq2}\right) / h_{eq} \tag{11}$$

where $L_{air\text{-}in}$ is the air-core inductance of the tertiary winding; $r_{eq2} = r + d_{02} + 0.5a_2$; and $A_{eq2} = r_{eq2}^2$. The value of L_{12} can be calculated using the following equation [27], [28]:

$$L_{12} = \frac{k_\rho \mu_0 N^2 \pi D_{12}}{h_{eq}} \left(\frac{a_1}{3} + d_{12} + \frac{a_2}{3}\right) = \frac{k_\rho \mu_0 N^2 \pi A_{eq12}}{h_{eq}} \tag{12}$$

where k_ρ is the Rogowski coefficient and $D_{12} = r_{eq1} + r_{eq2}$. From (12), because k_ρ is less than 1, $A_{eq1} > A_{eq2}$, $L_{air\text{-}out} > L_{air\text{-}in}$, $A_{eq1} > A_{eq12}$, and $L_{air\text{-}out} > L_{12}$. According to [29] and [30], $L_{air\text{-}in}$ is 0.5–1.0 times that of L_{12}, and $L_{air\text{-}out}$ is 1.5–2.0 times that of L_{12}.

D. Equivalent Model of Faulty Transformer

According to [31]–[35], internal faults in transformers can be analyzed using an additional winding connected in parallel to the faulty winding. Regardless of the fault type (turn-to-turn or turn-to-ground), in every equivalent model proposed in [31]–[35], the magnetizing branch of the faulty transformer is paralleled with the faulty winding.

To simplify the analysis, the fault diagram proposed in [32], [33], and [35] is used. When the fault is in winding 1, the transformer is equivalent to a three-winding autotransformer, as shown in Fig. 8, where the number of turns in winding 1 is denoted as

N_1 and that in the faulty winding *bc* is denoted as N_b. The short circuit turns ratio n_f is equal to the ratio of N_b to N_1. In [31] and [32], the calculations for the equivalent inductances of windings *ab* and *bc* are complex. However, because the fault winding (i.e., the common winding of the equivalent autotransformer shown in Fig. 8) is short-circuited, the magnetizing branch in the equivalent circuit of the faulty transformer is connected in parallel to the impedance of the faulty winding, as demonstrated by all the equivalent circuits displayed in [17], [34], and [35].

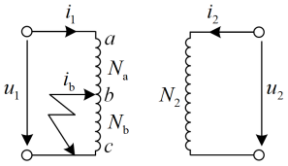

Fig. 8. Transformer fault diagram.

To simplify the analysis, the simplified equivalent model proposed in [35] shown in Fig. 9 is used. The inductance L_m represents the magnetizing branch, and the variables R_{sh} and L_{sh} are the equivalent reactance and inductance of the faulty arc, respectively.

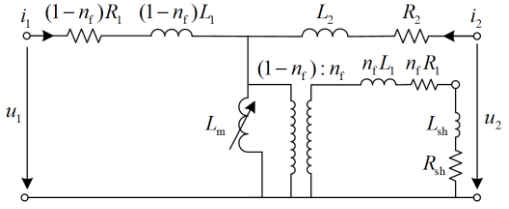

Fig. 9. Equivalent circuit of faulty transformer.

Based on the model shown in Fig. 9, we can evaluate two cases.

Case 1: The fault current is relatively large, so i_2 can be ignored, and $i_1 \approx i_d$. Furthermore, L_{eq} is relatively small if n_f is close to 1.

Case 2: If n_f is relatively small (i.e., during a minor turn-to-turn fault), the value of i_2 relative to the fault current cannot be neglected. However, in the case of a minor turn-to-turn fault, the terminal voltages of the transformer remain almost unchanged and $u_1 \approx u_2$. Therefore, u_1 and u_2 can also be connected in parallel to produce the model shown in Fig. 7.

A faulty transformer is equivalent to an autotransformer with a short-circuited common winding. Taking Fig. 9 as an example, due to the parallel connection of the inductance L_m and the inductance of the faulty winding, if calculated according to the model in Fig. 7, the inductance L_{eq} of the faulty transformer cannot exhibit the same high value as that of a healthy transformer with unsaturated iron, regardless of whether the core of the faulty transformer is saturated or not. Furthermore, when using the model shown in Fig. 7 to calculate the physical characteristics of a faulty transformer (based on either u_1 or u_2), the instantaneous value of L_{eq} should be stable because of the minimal influence of L_m. However, according to (5) and (7), the instantaneous value of L_{eq} during the transient period of the inrush current varies significantly between the saturated and unsaturated iron cores.

Moreover, when an internal fault occurs, because the steady-state waveforms of the winding voltage and differential winding current are both sinusoidal, the steady-state value of L_{eq} should be constant according to the model shown in Fig. 7. If each equivalent element shown in Fig. 9 is regarded as independent of the voltage and current, then L_{eq} should be independent of the external source.

III. Proposed Method

A. Algorithm of Equivalent Inductance

The unified transformer model (with or without an internal fault) is shown in Fig. 7, and the equation describing it is expressed as follows:

$$u_1 = R_{eq} i_d + L_{eq} \frac{\mathrm{d}i_d}{\mathrm{d}t} \tag{13}$$

Differential equations use the discrete sampling sequences of $u_1(k)$ and $i_d(k)$ to calculate the discrete sequences $R_{eq}(k)$ and $L_{eq}(k)$. The R-L algorithm [36], [37], which is used in the distance protection of transmission lines, can be employed, i.e.:

$$L_{eq}(k) = \frac{\Delta t}{2} \times \left| \frac{A(k) - B(k)}{C(k) - D(k)} \right| \tag{14}$$

where Δt is the sample interval; $A(k)$, $B(k)$, $C(k)$, and $D(k)$ are expressed as follows:

$$\begin{cases} A(k) = \left[u_1(k-1) + u_1(k)\right] \times \left[i_d(k-2) + i_d(k-1)\right] \\ B(k) = \left[u_1(k-1) + u_1(k-2)\right] \times \left[i_d(k) + i_d(k-1)\right] \\ C(k) = \left[i_d(k-1) + i_d(k-2)\right] \times \left[i_d(k) - i_d(k-1)\right] \\ D(k) = \left[i_d(k-1) + i_d(k)\right] \times \left[i_d(k-1) - i_d(k-2)\right] \end{cases} \tag{15}$$

According to [37], the R-L algorithm exhibits superior stability when the sampling frequency is between 1000 Hz and 2000 Hz, and it can effectively filter the DC component in the fault current.

In the unsaturated region of the inrush current, $i_d(k)$, $i_d(k-1)$, and $i_d(k-2)$ may all be approximately zero, and $\left(A(k) - B(k)/C(k) - D(k)\right)$ may be a negative

number with a large absolute value. Thus, the absolute value is used here.

B. Discrimination Scheme

The flowchart of the proposed discrimination scheme is shown in Fig. 10.

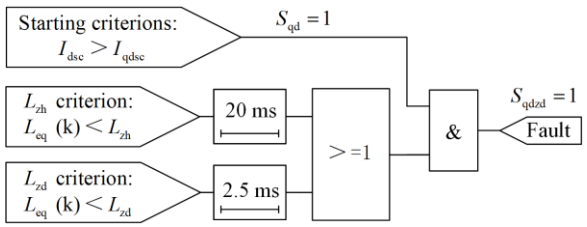

Fig. 10. Flowchart of the proposed discrimination scheme.

The starting criterion is expressed as follows:

$$I_{\mathrm{dsc}} > I_{\mathrm{qdsc}} \tag{16}$$

where I_{dsc} is the amplitude of i_{d} calculated via the half-wave integration algorithm; and I_{qdsc} is the threshold of the starting criterion. Accounting for the unbalanced current caused by the actual operating turn ratio, measurement noise, and tap position, I_{qdsc} is set to 0.2 times the rated current, and S_{qd} is the mark signal of the starting criterion.

When the core is fully saturated, the air-core inductance represents the lower limit of the equivalent winding inductance, and thus, L_{eq} must have a lower limit. In the proposed scheme, if $L_{\mathrm{eq}}(k)$ is continuously lower than the low threshold L_{zd} for m times, it is deemed an internal fault. As shown in Fig. 10, assuming a sampling frequency of 2000 Hz and $m = 5$, the L_{zd} criterion has a discrimination delay of 2.5 ms.

As shown in Fig. 10, the scheme defines a high threshold L_{zh}. For one cycle (20 ms for f = 50 Hz), if all the $L_{\mathrm{eq}}(k)$ values are less than L_{zh}, it is also regarded as an internal fault. In every cycle of the transient period of the inrush current, a discontinuous region exists, in which the transformer core is unsaturated. In this region, L_{m1} and L_{m2} are relatively large, while the calculated value of L_{eq} is significantly larger than L_{zh}, so it is evaluated as an inrush current according to the scheme. As shown in Fig. 10, the L_{zh} criterion has a discrimination delay of 20 ms, and S_{qdzd} is the discrimination mark signal.

C. Setting Principles

The setting principles of L_{zd} and L_{zh} are established as follows.

1) Low Threshold L_{zd}

First, to ensure that no judgment errors occur when the core is deeply saturated, the basic principle for setting L_{zd} requires it to be sufficiently small. Equation (7) indicates that L_{eq} is greater than $L_{\mathrm{m1}} // L_{\mathrm{m2}}$ when the core is saturated, and therefore, L_{zd} can be determined based on $L_{\mathrm{zd}} = L_{\mathrm{m1}} // L_{\mathrm{m2}}$. Second, when the core is fully saturated (i.e., its magnetic permeability is equal to μ_0), the corresponding L_{m1} and L_{m2} values can be used to calculate L_{zd}. However, accurately calculating L_{m1} and L_{m2} is nearly impossible. Nonetheless, in [29] and [30], it is found that $L_{\text{air-in}}$ is typically 0.5–1.0 times the value of L_{12} and that $L_{\text{air-out}}$ is typically 1.5–2.0 times the value of L_{12}. Therefore, if L_{m1} and L_{m2} are appropriately selected, while the values of $L_{\text{air-out}}$ and $L_{\text{air-in}}$ calculated according to (8) and (9), respectively, are smaller than the range of the air-core inductances recorded in [29] and [30], and L_{zd} is defined as $L_{\mathrm{zd}} = L_{\mathrm{m1}} // L_{\mathrm{m2}}$, then zero misjudgments can be theoretically guaranteed. Therefore, even if the permeability of the transformer core is equal to the vacuum permeability μ_0, the corresponding L_{m1} and L_{m2} values will not be lower than the corresponding L_{m1} and L_{m2} values of L_{zd}. Thus, equations $L_{\mathrm{m1}} = L_{12} = L_{\text{m1-sat}}$ and $L_{\mathrm{m2}} = 0.5L_{12} = L_{\text{m2-sat}}$ are defined. Using (8) and (9), $L_{\text{air-out}}$ and $L_{\text{air-in}}$ are $0.6L_{12}$ and $0.4L_{12}$, respectively, both being lower than the values provided in [29] and [30]. Accordingly, L_{zd} can be expressed as follows:

$$L_{\mathrm{zd}} = (0.5L_{12}L_{12})/(0.5L_{12} + L_{12}) = L_{12}/3 \tag{17}$$

2) High Threshold L_{zh}

In the case of a minor turn-to-turn fault, this threshold should be set with caution because the terminal voltage of the transformer is almost unchanged. Equation (13) assumes that:

$$u_1(t) = \sqrt{2}U_{\mathrm{N}}\sin(\omega t) \tag{18}$$

where U_{N} is the root mean square (RMS) value of the rated phase voltage.

By ignoring the possible DC component in the differential current i_{d} (owing to the filtering capacity of the R-L algorithm), there is:

$$i_{\mathrm{d}}(t) = \sqrt{2}kI_{\mathrm{N}}\sin(\omega t - \varphi) \tag{19}$$

where I_{N} is the RMS value of the rated current of the transformer; k is the coefficient; and φ is the angle at which i_{d} lags behind u_1.

Based on Fig. 3(f), φ can be expressed as follows:

$$\varphi = \arctan\left(\omega L_{\mathrm{eq}}/R_{\mathrm{eq}}\right) \tag{20}$$

Substituting (18)–(20) into (13) results in:

$$Z_{eq}=\sqrt{R_{eq}^2+\omega^2 L_{eq}^2}=U_N/(kI_N)=Z_N/k \tag{21}$$

where Z_N is the rated impedance of the transformer.

Furthermore, L_{eq} can be expressed as follows:

$$L_{eq}=(Z_N\sin\varphi)/(\omega k) \tag{22}$$

The coefficient k is set to 0.2. Thus, theoretically, L_{eq} is sensitive to any internal fault with a winding differential current of 0.2 times that of the rated current. In addition, φ is set to 90°, and the maximum L_{eq} is obtained after k has been determined. The high threshold L_{zh} is defined as follows:

$$L_{zh}=5Z_N/\omega \tag{23}$$

IV. Three-Phase Three-Winding Autotransformer

Extra-high voltage (EHV) three-phase transformers with large capacities comprise three single-phase three-winding autotransformers. The layout of these autotransformers, which consist of a core and windings, is shown in Fig. 11.

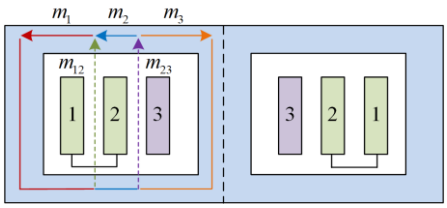

Fig. 11. Layout of single-phase three-winding autotransformer.

Autotransformers [38] can also be modeled using the duality principle. The original dual equivalent model of single-phase three-winding autotransformers is shown in Fig. 12(a), where L_{12} and L_{23} are the leakage inductance between windings 1 and 2, and windings 2 and 3, respectively, both variables can be obtained using the short circuit test parameters listed on the transformer nameplate; the nonlinear inductances L_{m1}, L_{m2}, and L_{m3} represent the equivalent inductances corresponding to the magnetic circuits m_1, m_2, and m_3 shown in Fig. 11, respectively.

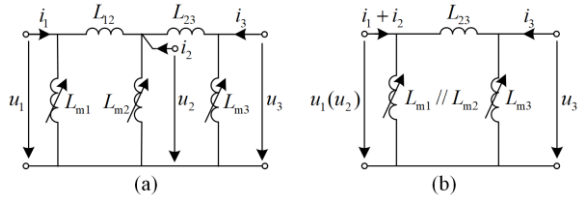

Fig. 12. Dual equivalent model of single-phase three-winding autotransformer. (a) Original model. (b) Transformed model.

Moreover, the magnetic leakages corresponding to the magnetic circuits m_{12} and m_{23}, shown in Fig. 11, are cross-linked (i.e., an equivalent mutual inductance between L_{12} and L_{23} exists). However, the effect of this mutual inductance is small, which is neglected in Fig. 12(a) for the analysis of L_{zd}.

Furthermore, u_1, u_2, and u_3 represent the voltages of series, common, and tertiary windings, respectively. During the inrush current period, when converted to the same winding via the transformation ratio, u_1 and u_2 are approximately equal because the series and common windings are connected. In addition, when a single-phase autotransformer is energized from the high-voltage (HV) side, $i_2=i_1$ and $i_3=0$.

Based on the same equivalent method shown in Figs. 1 and 3(a), and considering that $u_1\approx u_2$, the transformed equivalent model shown in Fig. 12(b) can be obtained. The winding differential current i_d is calculated as follows:

$$i_d=i_3+i_2+i_1 \tag{24}$$

The equivalent inductance L_{eq} of a three-winding autotransformer can be analyzed using Fig. 12(b) similar to that of Fig. 3. If the core is unsaturated and $u_1\approx u_2\approx u_3$, Fig. 12(b) can be analyzed similar to that of Figs. 3 and 5. If the core is saturated, $u_1\approx u_2$ and $u_1>u_3$, and Fig. 12(b) can be analyzed similar to that of Figs. 3 and 6.

As presented in Fig. 1 and expressed by (8) and (9), the model presented in Fig. 12(a) can be used to derive the equations expressed as follows:

$$L_{air\text{-}out}=2L_{m1\text{-}sat}//L_{m2\text{-}sat}//(L_{23}+L_{m3\text{-}sat}) \tag{25}$$

$$L_{air\text{-}com}=L_{m2\text{-}sat}//(L_{12}+L_{m1\text{-}sat})//(L_{23}+L_{m3\text{-}sat}) \tag{26}$$

$$L_{air\text{-}in}=L_{m3\text{-}sat}//\left[L_{23}+L_{m2\text{-}sat}//(L_{12}+L_{m1\text{-}sat})\right] \tag{27}$$

where $L_{air\text{-}com}$ is the air-core inductance of the common winding; while $L_{m1\text{-}sat}$, $L_{m2\text{-}sat}$, and $L_{m3\text{-}sat}$ are the values of L_{m1}, L_{m2}, and L_{m3} respectively, when the core is fully saturated. Moreover, the analysis of $L_{air\text{-}out}$ in (25) is different from that of $L_{air\text{-}com}$ and $L_{air\text{-}in}$ in (26) and (27) because $i_2=i_1$ when i_1 is injected to the series winding of the autotransformer.

According to (27), if $L_{m3\text{-}sat}=0.5L_{23}$, then $L_{air\text{-}in}$ is less than $0.5L_{23}$. According to (26), if $L_{m2\text{-}sat}=L_{23}$, then $L_{air\text{-}com}$ is less than L_{23}. As discussed in [29], the air-core inductance of a two-winding autotransformer should be higher than its leakage inductance. Thus, according to (25), if $L_{m1\text{-}sat}=L_{12}/3$, then $L_{air\text{-}out}$ is less than L_{12}. Therefore, L_{m1}, L_{m2}, and L_{m3} are assigned values of $L_{12}/3$, L_{23}, and $0.5L_{23}$, respectively. Similar to the analysis of L_{zd} in (17), the value of L_{zd} for the three-winding autotransformer can be set to $(L_{m1}//L_{m2})//L_{m3}$, i.e.:

$$L_{zd}=(L_{12}/3)//L_{23}//(0.5L_{23})=L_{12}L_{23}/(3L_{12}+3L_{23}) \tag{28}$$

In addition, the high threshold L_{zh} of a three-winding autotransformer can be defined according to (23).

V. Simulations and Recorded Data Tests

A. PSCAD Simulations

A single-line diagram of the simulation model constructed using PSCAD is shown in Fig. 13. The specifications of the simulation model are detailed in Appendix A. To simulate internal faults, the simulation methods presented in [39] and [40] are followed using three single-phase four-winding transformer models to form a YNd11 three-phase transformer. Turn-to-turn and turn-to-ground faults are modeled in the 500 kV winding of Phase A. Following [41] and [42], the short arc is modeled using a resistance R_{sh} in series with an inductance L_{sh}. Additionally, a duality-based, three-phase, two-winding transformer model is used to simulate inrush currents. The duality-based model in PSCAD is detailed in [43].

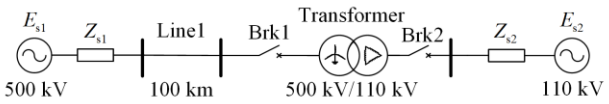

Fig. 13. Single-line diagram of simulation model.

According to the setting principle, for converting to the HV side, L_{zd} and L_{zh} are set to 0.0688 H and 7.37 H, respectively. The sampling frequency is set to 2000 Hz, and m is set to 5 for the scheme. The inrush current, turn-to-turn faults, and turn-to-ground faults are simulated as follows.

1) Inrush Current

Based on the critical saturation conditions of the core described in [44], the core remanence is set to 0.8 times that of the rated flux. Subsequently, as shown in Fig. 13, Brk2 is open, and Brk1 is switched on at 1.0 s, at which time the HV winding voltage u_{Ha} starts alternating across the zero point. The test results are shown in Fig. 14, in which u_{La} denotes the voltage of the low-voltage (LV) winding.

Figures 14(b) and (d) show the waveforms of u_{Ha} and u_{La}, and the inrush current from 1.035 s to 1.075 s, respectively. As seen, when the core is unsaturated from 1.0375 s to 1.043 s, u_{Ha} and u_{La} are approximately equal, and when the core is saturated from 1.043 s to 1.057 s, u_{Ha} is greater than u_{La}. Figures 14(b) and (d) verify the analysis of u_1 and u_2 presented in Section II. B.

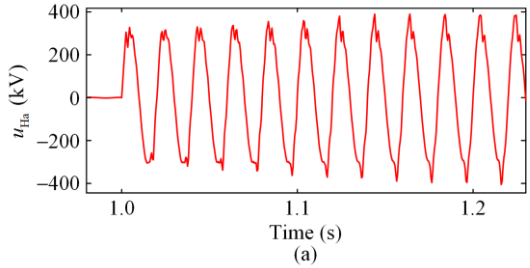

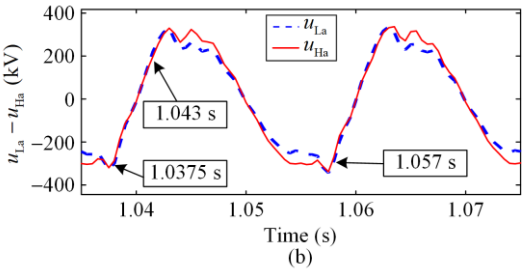

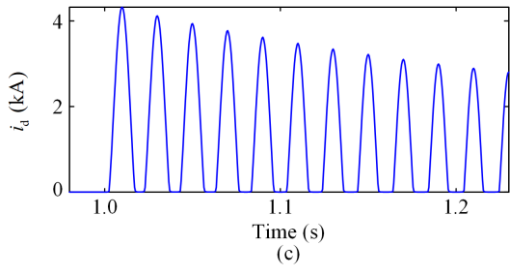

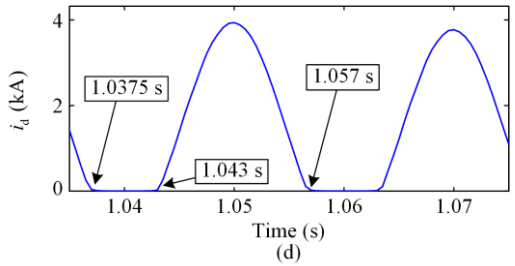

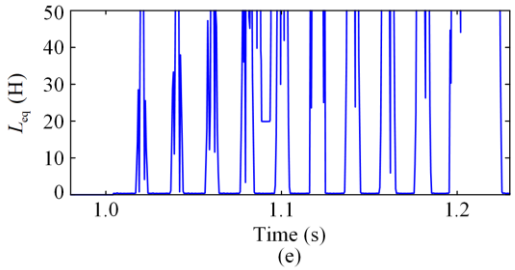

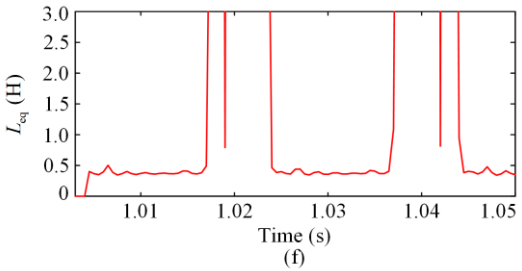

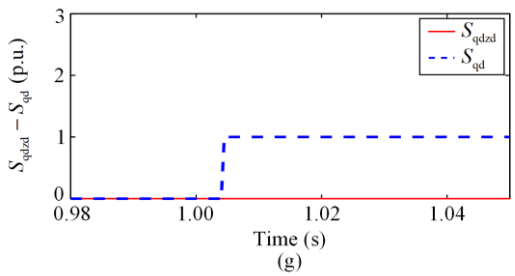

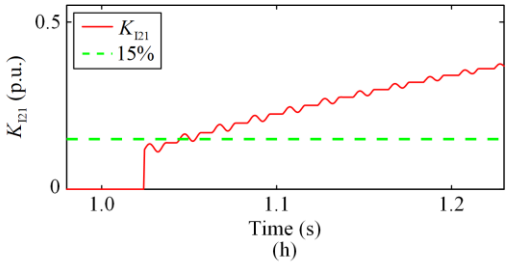

Fig. 14. Results of inrush current simulations. (a) Voltage of HV winding. (b) Local waveforms of HV and LV winding voltages. (c) Differential current i_d. (d) Local waveform of i_d. (e) Equivalent inductance L_{eq}. (f) Local waveform of L_{eq}. (g) Mark signals. (h) K_{I21} of i_d.

According to the i_d waveform shown in Fig. 14(c), the saturation is significant, and the dead angles are relatively small. As shown in Fig. 14(h), the ratio (K_{I21}) of the amplitude of the second harmonic of the inrush current to the amplitude of its fundamental wave is less than 15% in the transient period. Hence, for the methods based on the second harmonic restraint, this may result in an inaccurate evaluation.

The L_{eq} waveform based on u_{Ha} and i_d is shown in Fig. 14(e). As seen, the instantaneous values of L_{eq} exceeds L_{zh} in every unsaturated region after the starting criterion is activated. Figure 14(f) shows the L_{eq} waveform corresponding to the first sharp wave of i_d, where all instantaneous values of L_{eq} exceed L_{zd}. As shown in Fig. 14(g), S_{qdzd} remains equal to zero after S_{qd} is enabled, and the proposed method achieves accurate discrimination.

2) Turn-to-turn Fault

With a rated load of 65%, a 2% turn-to-turn fault is simulated at 1.0 s, and the results are shown in Fig. 15.

According to Fig. 15(b), the rms value of i_d is approximately 0.48 times that of the transformer's rated current. All the instantaneous values of L_{eq} are lower than L_{zh} 20 ms after the starting criterion is activated. The mark signals S_{qdzd} and S_{qd} shown in Fig. 15(d) demonstrate that the proposed method can accurately distinguish the currents.

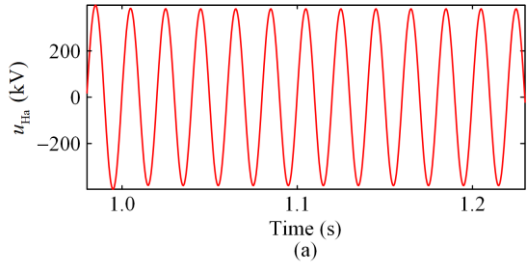

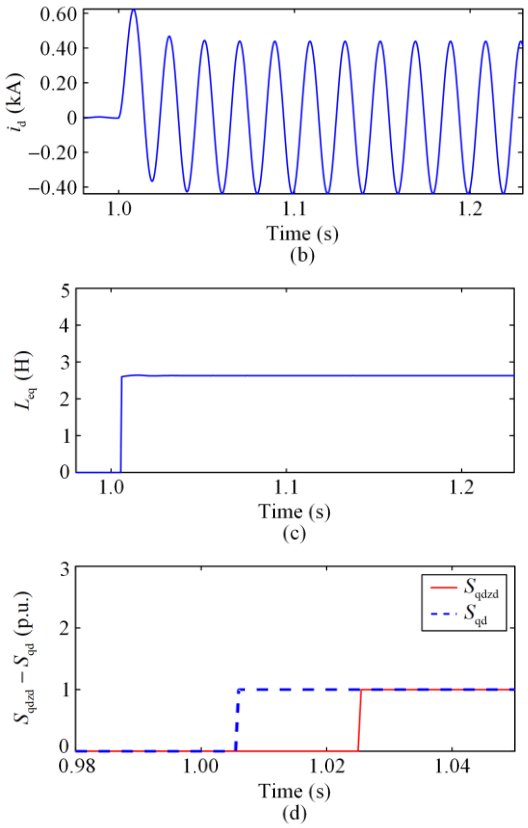

Fig. 15. Results of 2% turn-to-turn fault simulation. (a) HV winding voltage. (b) Differential current. (c) Equivalent inductance L_{eq}. (d) Mark signals.

3) Turn-to-ground Fault

With a rated load of 65 %, a turn-to-ground fault is simulated at 1.0 s, and the results are shown in Fig. 16. The ratio of the number of *bc* turns to that of *ac* turns is 48%, as reflected in Fig. 8.

The stable RMS value of i_d is 7.59 times the rated current of the transformer. As shown in Fig. 16(c), the stable value of L_{eq} is sufficiently small to enable rapid discrimination between the currents 2.5 ms after the starting criterion is activated.

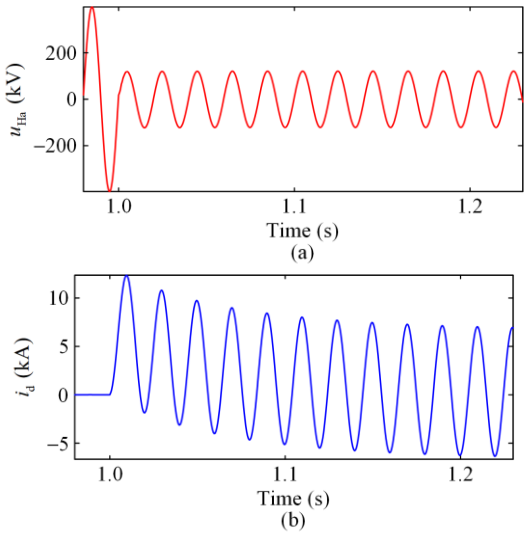

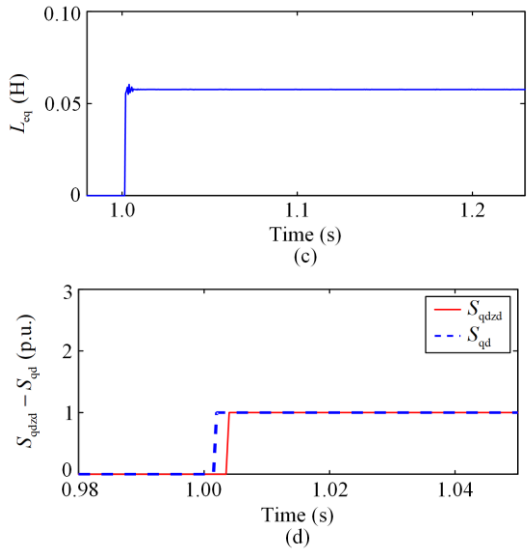

Fig. 16. Results of turn-to-ground fault simulation. (a) HV winding voltage. (b) Differential current. (c) Equivalent inductance L_{eq}. (d) Mark signals.

An additional simulation is conducted by tripling the source impedance of E_{s1} and the length of line 1, and the results are displayed in Fig. 17. As seen, the stable rms value of i_d is 3.96 times the rated current of the transformer. Compared with the waveforms shown in Fig. 16, the amplitude of i_d decreases while the stable value of L_{eq} remains unchanged. As shown in Fig. 17(d), the proposed method quickly identifies the fault. Furthermore, it is less influenced by the source equivalent impedance.

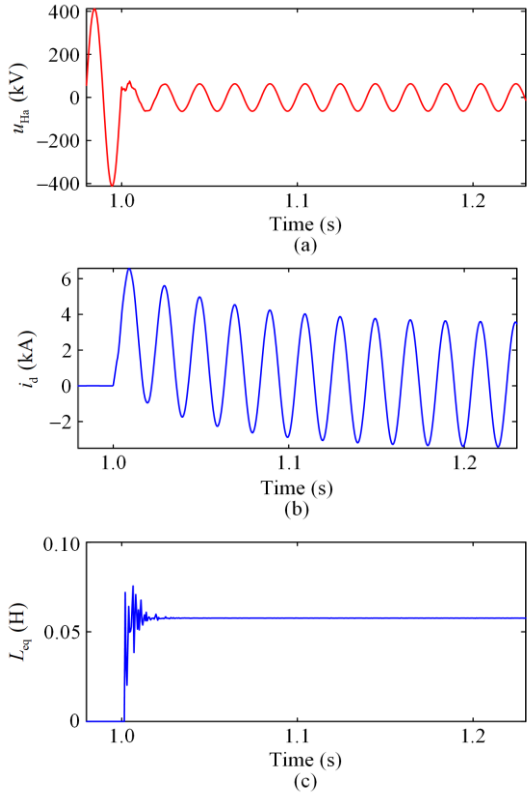

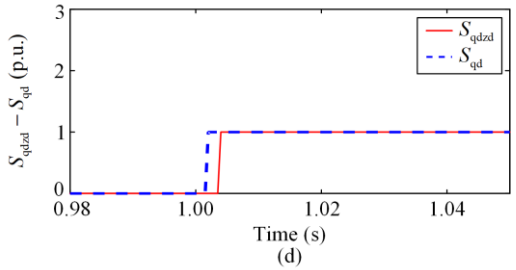

Fig. 17. Results of turn-to-ground fault simulation. (a) HV winding voltage. (b) Differential current. (c) Equivalent inductance L_{eq}. (d) Mark signals.

B. Tests of Dynamic Model Using Recorded Data

The proposed method is verified using the internal faults and inrush current in a three-winding autotransformer based on transformer protection data recorded during physical dynamic model tests. The specifications of the physical dynamic model are detailed in Appendix B. According to the setting principle, for converting to the HV side, L_{zd} and L_{zh} are set to 0.032 H and 5.31 H, respectively. Voltage transformers are installed on busbars 1 and 2, as shown in Fig. B1 in Appendix B. The value of L_{eq} is calculated using the HV winding voltage, the sampling frequency is set to 2000 Hz, and m is set to 5 for the discrimination criterion.

1) Inrush Current

The transformer is energized at the 500 kV side. As shown in Figs. 18(a) and (c), for Phase A of the transformer, the peak value of i_d is five times rated transformer current, and the corresponding instantaneous L_{eq} value is 0.0603 H, which is the minimum of all the instantaneous values of L_{eq}. The waveform of L_{eq} does not satisfy the requirements of the quick discrimination criterion. As shown in Fig. 18(d), the proposed method accurately distinguishes the currents.

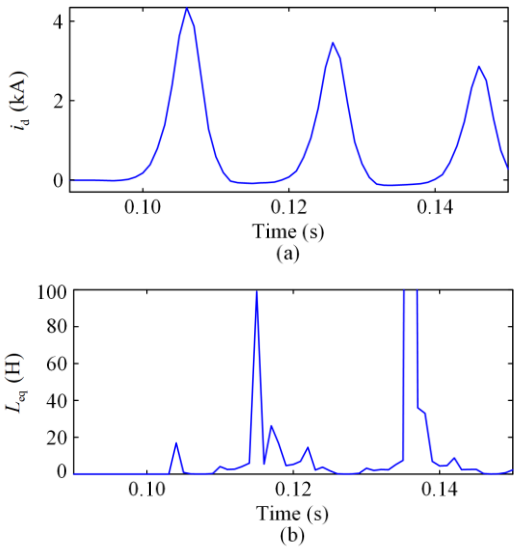

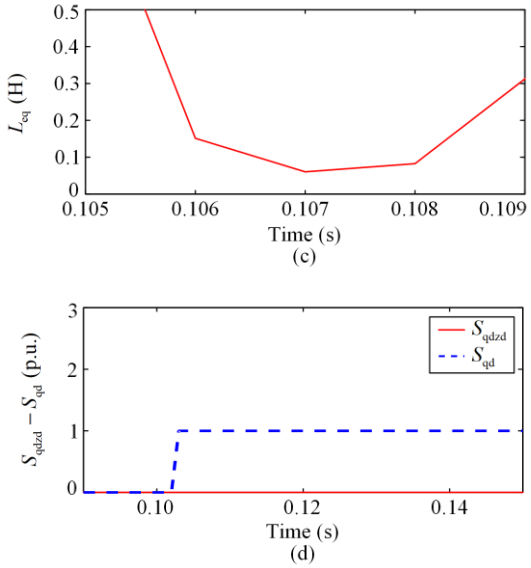

Fig. 18. Test results of inrush current. (a) HV winding voltage. (b) Differential current. (c) Equivalent inductance L_{eq}. (d) Mark signals.

2) Turn-to-turn Fault

When the experimental autotransformer is operating at 60% of the rated load, a 2% turn-to-turn fault is activated in the series winding of Phase A at 0.1 s. The test results are shown in Fig. 19. The proposed method accurately discriminates the currents 20 ms after the starting criterion is activated, as shown in Fig. 19(d).

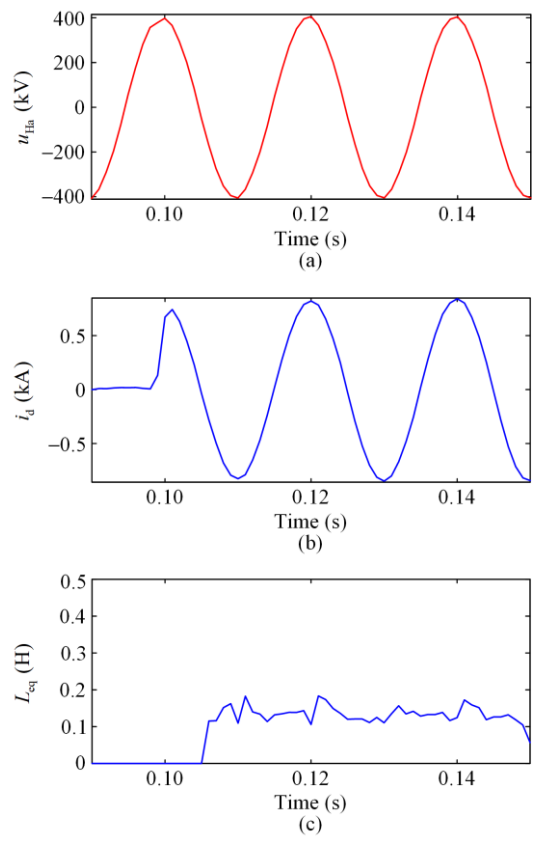

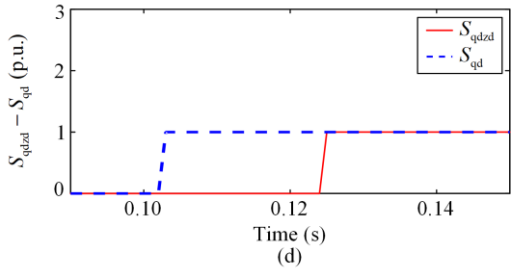

Fig. 19. Test results of 2% turn-to-turn fault in series winding. (a) HV winding voltage. (b) Differential current. (c) Equivalent inductance L_{eq}. (d) Mark signals.

3) Phase-to-ground Fault of Lead Wire

A fault is introduced in the lead wire of the HV winding for Phase A, and the test results are shown in Fig. 20. As seen from the mark signals shown in Fig. 20(d), the proposed method quickly and accurately discriminates the currents 2.5 ms after the starting criterion is activated.

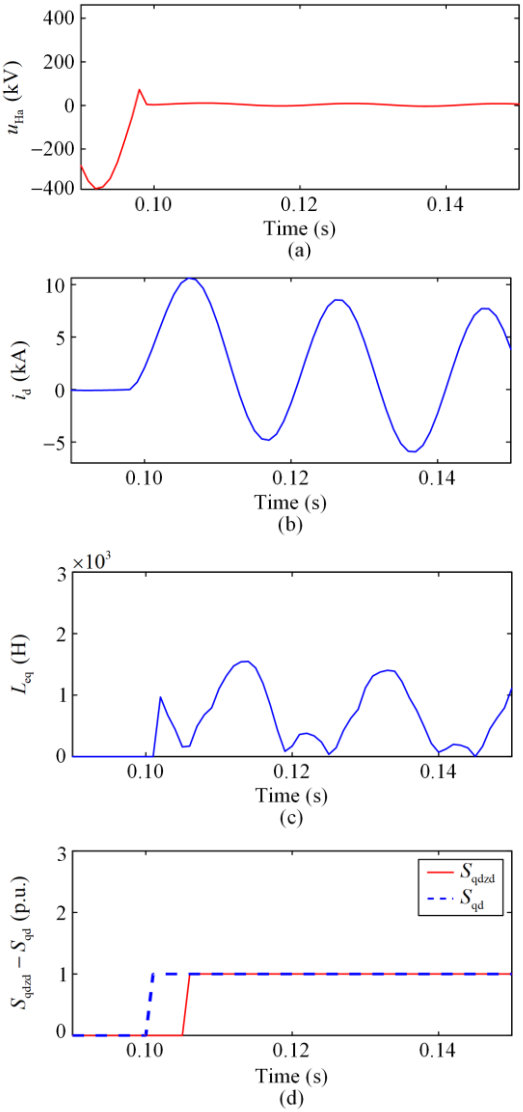

Fig. 20. Test results of phase-to-ground fault in HV lead wire. (a) HV winding voltage. (b) Differential current. (c) Equivalent inductance L_{eq}. (d) Mark signals.

4) Energizing Transformer with Internal Fault

At 0.1 s, the transformer is energized from the HV winding, and at 0.16 s, a 2% turn-to-turn fault occurred in Phase B. The test results are shown in Fig. 21, in which u_{Hb} and i_{d} denote the winding voltage and differential current of phase B, respectively. As indicated by the mark signals in Fig. 21(d), the starting criterion is activated immediately after the energization, and the proposed method successfully identifies the internal fault at 0.18 s.

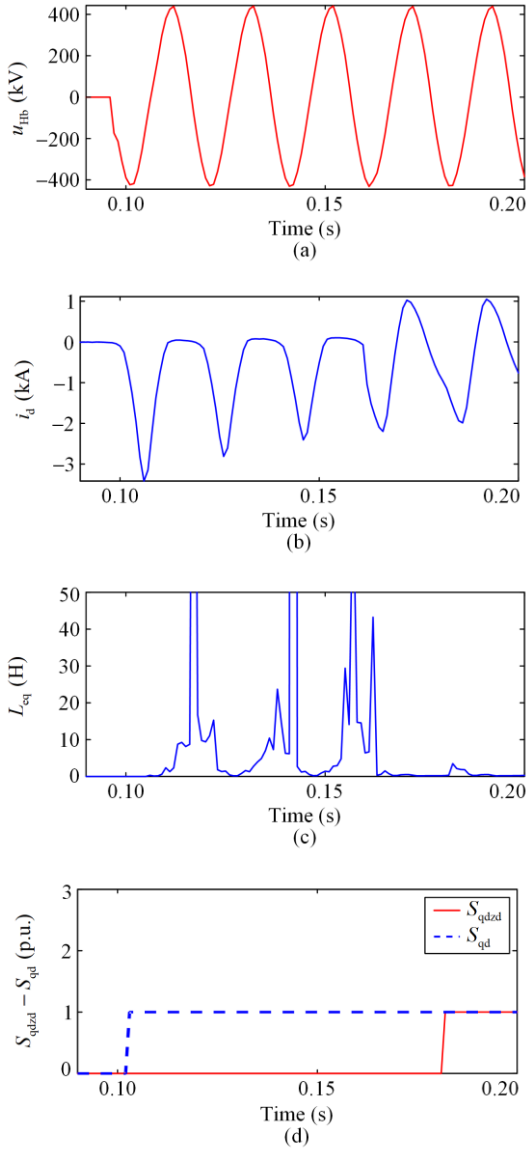

Fig. 21. Test results of inrush current with 2% turn-to-turn fault. (a) HV winding voltage. (b) Differential current. (c) Equivalent inductance L_{eq}. (d) Mark signals.

C. Test of Field Transformer Using Recorded Data

The proposed method is verified using the transformer protection data recorded for a 500 kV three-winding autotransformer. The winding connection for the 500/220/35 kV transformer is YnYnd11, and the rated capacity is 1002 MVA. The leakage reactance X_{1-2}, X_{1-3}, and X_{1-3} of the transformer are 0.177 p.u., 0.599 p.u., and 0.392 p.u., respectively. According to the setting principle, L_{zd} and L_{zh} are set to 0.032 H and 3.973 H, respectively.

The transformer is energized from the 220 kV winding, and the breakers of the 500 kV and 35 kV sides are open. The test results for the inrush current are shown in Fig. 22. The differential winding current of Phase C and the corresponding K_{I21} values are shown in Figs. 22(c) and (h), respectively. K_{I21} is less than 15% during the transient period, indicating that the core of Phase C is deeply saturated.

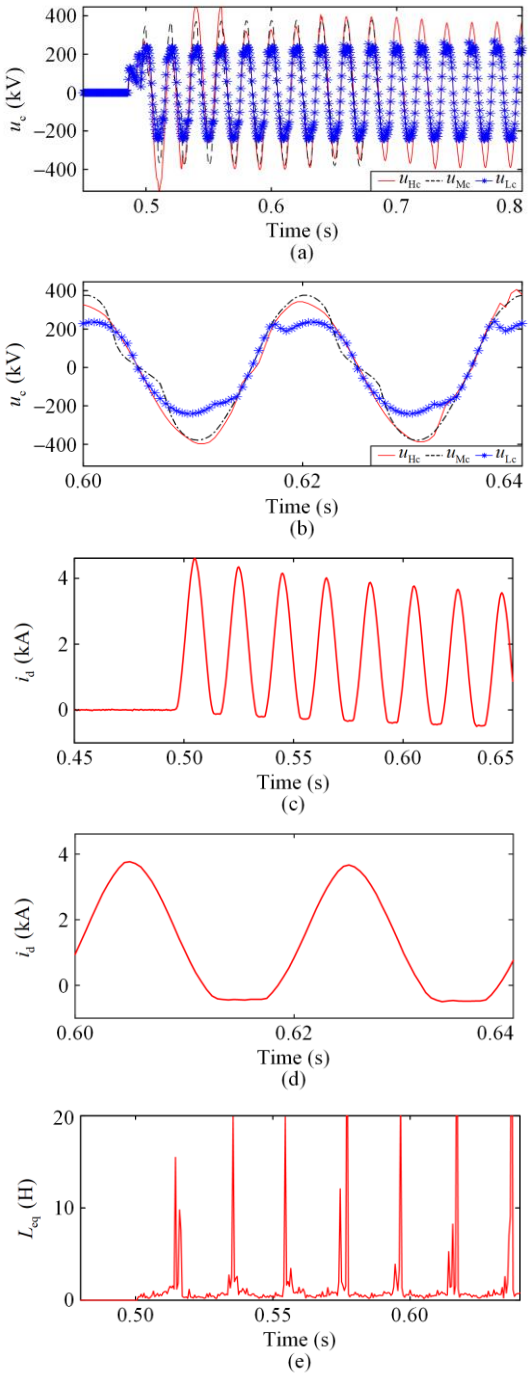

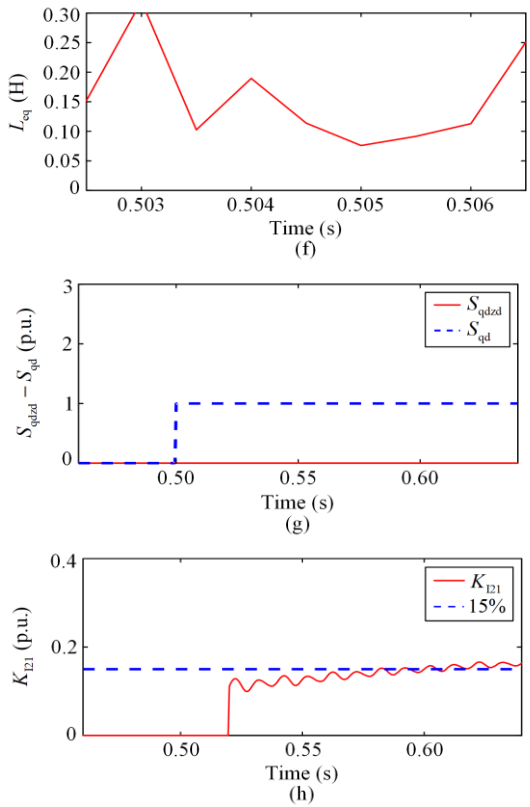

Fig. 22. Test results for inrush current in 500 kV autotransformer using transformer protection data. (a) Voltages of HV, common, and tertiary winding. (b) Local waveforms of HV, common, and tertiary winding voltages. (c) Differential current i_d. (d) Local waveform of i_d. (e) Equivalent inductance L_{eq}. (f) Local waveform of L_{eq}. (g) Mark signals. (h) K_{I21} of i_d.

Unlike general field transformers, voltage transformers are typically installed on the lead wires on each side of the autotransformer. Accordingly, for Phase C, when energizing from the 220 kV side, the HV winding voltage u_{Hc}, common winding voltage u_{Mc}, and tertiary winding voltage u_{Lc} are all measured, as shown in Figs. 22(a) and (b). When the core is unsaturated, u_{Hc}, u_{Mc}, and u_{Lc} are approximately equal. Conversely, when the core is saturated, u_{Lc} is less than both u_{Hc} and u_{Mc}, and the latter two remain approximately equal. The results for L_{eq} calculated using u_{Mc} and i_d are shown in Figs. 22(e) and (f). According to the values of S_{qdzd} in Fig. 22(g) and K_{I21} in Fig. 22(h), the proposed method delivers accurate assessments during the transient period when K_{I21} is lower than 15%.

VI. Conclusion

Accurately and quickly discriminating between inrush and fault currents in power transformers is important for their protection. Based on the dual equivalent model of a single-phase two-winding transformer and a single-phase three-winding autotransformer, this paper proposes a method that discriminates inrush currents from internal fault current using the equivalent inductance of the dual model.

PSCAD simulations and recorded transformer protection data demonstrate that the method can accurately identify inrush current when the transformer core is deeply saturated, and can rapidly discriminate between currents when a critical internal fault occurs. The PSCAD simulations also show that the proposed method is sensitive to minor internal faults but less sensitive to the equivalent impedance of the system.

The proposed method is applicable to three-phase transformer banks consisting of three single-phase transformers with independent magnetic circuits. Future studies will examine the influence of the saturation characteristics of the current transformer on the method, and investigate the application of the proposed method to three-phase multi-limb transformers.

Appendix A

The specifications of the PSCAD simulation system are shown in Table AI.

TABLE AI
Specifications of PSCAD Simulation System

Scheme		Parameter
Source Es1		Positive sequence impedance: $20\angle 85°\ \Omega$ Zero sequence impedance: $25\angle 85°\ \Omega$
Source Es2		Positive sequence impedance: $30\angle 80°\ \Omega$ Zero sequence impedance: $30\angle 80°\ \Omega$
Line		Simulation model: Bergeron model Positive sequence resistance: 0.0196 Ω/km Positive sequence inductance: 0.8917 mH/km Positive sequence impedance: 0.001 23 μF/km Zero sequence resistance: 0.1828 Ω/km Zero sequence inductance: 2.739 mH/km Zero sequence impedance: 0.000 84 μF/km
Duality-based three-phase two-winding transformer model	Basic parameters	YN/d11 connection; $S_{rated} = 540$ MVA Core model: three-phase bank Leakage reactance: 0.14 p.u.
	Saturation parameters	Magnetization model: basic hysteresis Knee voltage: 1.14 p.u. Magnetizing current: 1% p.u. Air-core reactance LA: 0.2 p.u. Loop width: 10%
Four-winding transformer model		YN/d11 connection; $S_{rated} = 540$ MVA Leakage reactance: 0.14 p.u.
		Fault arc: $R_{sh} = 0.1\ \Omega$; $L_{sh} = 1$ mH
Simulation settings		Time step: 25 μs Sampling frequency: 2000 Hz
Threshold settings		$Z_N = 500 \times 500 / 540 = 462.96\ \Omega$ $L_{zd} = 0.14 Z_N / (3 \times 314) = 0.0688$ H $L_{zh} = 5 Z_N / 314 = 7.37$ H

Figure A1 shows the core saturation characteristics, where λ and i are the magnetizing flux and current, respectively. The air-core reactance (inductance), denoted as L_A, is the minimum value of the slope of the curve, which is approximately twice the leakage reactance as discussed in [29]. The knee point of the satu-

ration curve, denoted as (λ_M, i_M), is expressed as a percent or per unit of the operating point, which is defined as the rated voltage. A typical per unit range for this knee point is 1.15 to 1.25.

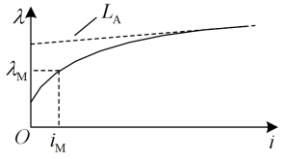

Fig. A1. Core saturation characteristics used in PSCAD simulations.

APPENDIX B

Figure B1 shows the physical dynamic model system. Three single-phase autotransformers are connected to model a 500 kV autotransformer with four fault setting points. In particular, turn-to-ground faults are not routine items; thus, they are replaced by phase-to-ground faults in the lead wire. The specifications of the dynamic model system are shown in Table BI.

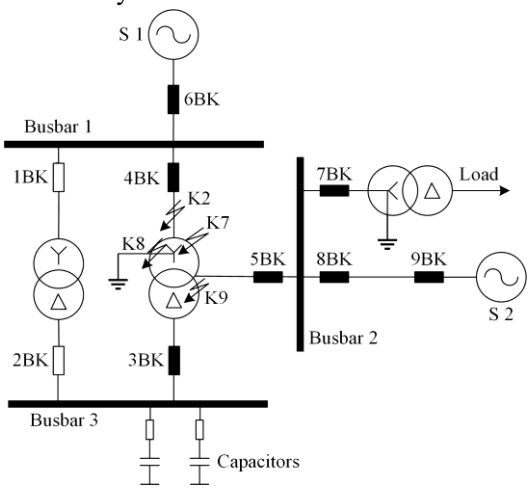

Fig. B1. Physical dynamic model system.

TABLE BI
SPECIFICATIONS OF DYNAMIC MODEL SYSTEM

Scheme		Parameter
Experimental transformer		Voltage ratio: 1400 V/600 V/99 V, YN/YN/d11 connection
Fault setting points	K2	Phase-to-ground fault in the HV lead wire
	K7	Turn-to-turn fault in the series winding
	K8	Turn-to-turn fault in the common winding
	K9	Turn-to-turn fault in the tertiary winding
Model ratio		Voltage: K_V=500000/1400; current: K_i=1250/5
Prototype 500 kV autotransformer		Voltage ratio: 500 kV/230 kV/36 kV YN/YN/d11 connection, S_{rated} = 750 MVA Leakage reactance: X1-2(%): 12.7; X1-3(%): 45.8; X2-3(%): 30.6
Prototype source and capacitors		S_1 = 10000 MVA ; S_2 = 1000 MVA capacity of capacitors: 225 Mvar
Threshold settings		$Z_N = 500 \times 500/750 = 333.33\ \Omega$ $L_{zd} = \frac{12.7\% \times 30.6\%}{12.7\% + 30.6\%} \times Z_N/(3 \times 314) = 0.0317$ H $L_{zh} = 5Z_N/314 = 5.31$ H

ACKNOWLEDGMENT

Not applicable.

AUTHORS' CONTRIBUTIONS

Jimin Chai: conceptualization, formal analysis, methodology, software, validation, and writing-original draft. Yuping Zheng: project administration and resources. Shuyan Pan: data curation, project administration (equal), software, and validation. All authors read and approved the final manuscript.

FUNDING

This work is supported by the National Natural Science Foundation of China (No. U1866603) and the Headquarters Technology Project of the State Grid Corporation of China (No. 5100-202340030A-1-1-ZN).

AVAILABILITY OF DATA AND MATERIALS

Not applicable.

DECLARATIONS

Competing interests: The authors declare that they have no known competing financial interests or personal relationships that could have appeared to influence the work reported in this article.

AUTHORS' INFORMATION

Jimin Chai received a B.S. degree from Xi'an Jiaotong University, Xi'an, China, in 2004 and an M.S. degree from the State Grid Electric Power Research Institute, Nanjing, China, in 2007, and a Ph.D. degree from Hohai University, Nanjing, China in 2025. Since 2009, he has been a lecturer at the School of Electrical and Information Engineering, Changzhou Institute of Technology, Changzhou, China. His research interests include power-system protection and control.

Yuping Zheng received a B.S. degree from Hefei University of Technology, Hefei, China in 1983, an M.S. degree from the Nanjing Electric Power Automation Research Institute, Nanjing, China in 1986, and a Ph.D. degree from Wuhan University, Wuhan, China in 2004. He is currently with the NARI Group Corporation (State Grid Electric Power Research Institute) and is an adjunct professor at Hohai University. His research interests include power-system protection and control.

Shuyan Pan received her B.S. and M.S. degrees from Hefei University of Technology, Hefei, China, in 1994 and 1997, respectively. She is currently a senior engineer at the NARI Group Corporation (State Grid Electric Power Research Institute). Her research interests include power-system protection and control.

REFERENCES

[1] IEEE Guide for Protecting Power Transformers, IEEE Std C37.91, 2021.

[2] S. Krishnamurthy and B. E. Baningobera, "IEC61850 standard-based harmonic blocking scheme for power transformers," *Protection and Control of Modern Power Systems*, vol. 4, no. 2, pp. 121-135, Apr. 2019.

[3] Y. Zhao and P. Crossley, "Countermeasure to prevent the incorrect blocking of differential protection applied to converter transformers," *IEEE Transactions on Power Delivery*, vol. 35, no. 1, pp. 95-105, Feb. 2020.

[4] J. Xia, Y. Fang, and B. Liu *et al*., "The transformer differential protection method based on characteristic current waveform width criterion," *Electric Power Engineering Technology*, vol. 39, no. 1, pp. 184-190, Jan. 2020. (in Chinese)

[5] Y. Zhang, J. Huang, and Y. Zhang *et al*., "High order statistical theory for identifying transformer inrush current by using dual characteristics," *Power System Protection and Control*, vol. 49, no. 24, pp. 21-30, Dec. 2021. (in Chinese)

[6] S. Afrasiabi, M. Afrasiabi, and B. Parang *et al*., "Designing a composite deep learning based differential protection scheme of power transformers," *Applied Soft Computing Journal*, vol. 87, Feb. 2020.

[7] Z. Li, Z. Jiao, and A. He, "Knowledge-based artificial neural network for power transformer protection," *IET Generation Transmission & Distribution*, vol. 14, no. 7, pp. 5782-5791, Aug. 2020.

[8] S. K. Murugan, S. P. Simon, and R. R. Eapen, "A novel signal localized convolution neural network for power transformer differential protection," *IEEE Transactions on Power Delivery*, vol. 37, no. 2, pp. 1242-1251, Apr. 2022.

[9] Z. Li, Z. Jiao, and A. He, "Dynamic differential current-based transformer protection using convolutional neural network", *CSEE Journal of Power and Energy Systems*, vol. 11, no. 2, pp. 871-885, May 2022. (in Chinese)

[10] K. Yabe, "Power differential method for discrimination between fault and magnetizing inrush current in transformers," *IEEE Transactions on Power Delivery*, vol. 12, no. 3, pp. 1109-1118, Jul. 1997.

[11] Y. Zheng, X. Liu, and Y. Bo *et al*., "A method of adaptive transformer turn-turn fault protection based on power loss," *Automation of Electric Power Systems*, vol. 37, no. 10, pp. 104-107, Jul. 2013. (in Chinese)

[12] R. P. Medeiros and F. B. Costa, "A wavelet-based transformer differential protection: internal fault detection during inrush conditions," *IEEE Transactions on Power Delivery*, vol. 33, no. 6, pp. 2965-2977, Dec. 2018.

[13] M. O. Oliveira, A. S. Bretas, and G. D. Ferreira, "Adaptive differential protection of three-phase power transformers based on transient signal analysis," *International Journal of Electrical Power & Energy Systems*, vol. 57, pp. 366-374, May 2014.

[14] A. Roy, R. K. Misra, and D. Singh *et al*., "Differential protection scheme for power transformers using matched wavelets," *IET Generation Transmission & Distribution*, vol. 13, no. 12, pp. 2423-2437, Jun. 2019.

[15] A. Behvandi, S. G. Seifossadat, and A. Saffarian, "A new method for discrimination of internal fault from other transient states in power transformer using Clarke's transform and modified hyperbolic S-transform," *Electric Power Systems Research*, vol. 178, pp. 106023-106023, Jan. 2020.

[16] A. G. Phadke and J. S. Thorp, "A new computer-based flux-restrained current-differential relay for power transformer protection," *IEEE Transactions on Power Apparatus and Systems*, vol. 102, no. 11, pp. 3624-3629, Nov. 1983.

[17] B. Ge, A. T. de Almeida, and Q. Zheng *et al*., "An equivalent instantaneous inductance-based technique for discrimination between inrush current and internal faults in power transformers," *IEEE Transactions on Power Delivery*, vol. 20, no. 4, pp. 2473-2482, Oct. 2005.

[18] K. Inagaki, M. Higaki, and Y. Matsui *et al*., "Digital protection method for power transformers based on an equivalent circuit composed of inverse inductance," *IEEE Transactions on Power Delivery*, vol. 3, no. 4, pp. 1501-1510, Oct. 1988.

[19] Z. Hao, B. Zhang, and Y. Chu *et al*., "Study on transformer protection principle based on equivalent circuit equilibrium equation," *Proceedings of the CSEE*, vol. 26, no. 10, pp. 67-72, Oct. 2006. (in Chinese)

[20] W. X. Sima, Y. Liu, and M. Yang *et al*., "An improved π model for single-phase two winding transformers considering deep saturation of the iron core," *Proceedings of the CSEE*, vol. 38, no. 24, pp. 7131-7140, Dec. 2018. (in Chinese)

[21] S. Jazebi, S. E. Zirka, and M. Lambert, *et al*., "Duality derived transformer models for low-frequency electromagnetic transients Part I topological models," *IEEE Transactions on Power Delivery*, vol. 31, no. 5, pp. 2410-2419, Oct. 2016.

[22] S. Jazebi, A. Rezaei-Zare, and M. Lambert *et al*., "Duality-derived transformer models for low-frequency electromagnetic transients Part II Complementary modeling guidelines," *IEEE Transactions on Power Delivery*, vol. 31, no. 5, pp. 2420-2430, Oct. 2016.

[23] F. D. Leon, A. Farazmand, and P. Joseph, "Comparing the T and π equivalent circuits for the calculation of transformer inrush currents," *IEEE Transactions on Power Delivery*, vol. 27, no. 4, pp. 2390-2398, Oct. 2012.

[24] S. Jazebi, F. D. Leon, and A. Farazamand *et al*., "Dual reversible transformer model for the calculation of low-frequency transients," *IEEE Transactions on Power Delivery*, vol. 28, no. 4, pp. 2509-2517, Oct. 2013.

[25] S. E. Zirka, Y. I. Moroz, and C. M. Arturi *et al*., "Topology-correct reversible transformer model," *IEEE Transactions on Power Delivery*, vol. 27, no. 4, pp. 2037-2045, Oct. 2012.

[26] M. Lambert, D. M. Martinez, and J. Mahseredjian *et al*., "Transformer leakage flux models for electromagnetic transients: critical review and validation of a new model," *IEEE Transactions on Power Delivery*, vol. 29, no. 5, pp. 2180-2188, Oct. 2014.

[27] F. D. Leon, and J. A. Martinez. "Dual three-winding transformer equivalent circuit matching leakage meas-

urements." *IEEE Transactions on Power Delivery*, vol. 24, no. 1, pp. 160-168, Jan. 2009.

[28] K. N. Yin, "Short circuit impedance calculation," in *Transformer Design Principle*, Beijing, China: Chinese Power Press, 2003, pp. 195-214. (in Chinese)

[29] H. W. Dommel, "Transformers," in *EMTP Theory Book*, 2nd ed, Microtran Power System Analysis Corporation, 1996, pp. 210-220.

[30] S. W. Shi, "Internal fault and over excitation protection of transformers," in *Relay Protection of Large Generator Unit*, Beijing, China: Water Resources and Electric Power Press, 1987, pp. 153-156. (in Chinese)

[31] P. Bastard, P. Bertrand, and M. Meunier, "A transformer model for winding fault studies," *IEEE Transactions on Power Delivery*, vol. 9, no. 2, pp. 690-699, Apr. 1994.

[32] L. M. R. Oliveira and A. J. M. Cardoso, "Leakage inductances calculation for power transformers interturn fault studies," *IEEE Transactions on Power Delivery*, vol. 30, no. 3, pp. 1213-1220, Jun. 2015.

[33] A. Berzoy, A. A. 1 S. Mohamed, and O. A. Mohammed, "Inter-turn short-circuit fault model for magnetically coupled circuits: a general study," in *2016 IEEE Industry Applications Society Annual Meeting*, Portland, USA, Oct. 2016, pp. 1-7.

[34] N. Asadi and H. M. Kelk, "Modeling, analysis, and detection of internal winding faults in power transformers," *IEEE Transactions on Power Delivery*, vol. 30, no. 6, pp. 2419-2426, Dec. 2015.

[35] H. Hua, D. You, and Y. Wang *et al.*, "Performance analysis and criterion improvement for transformer protection theory based on transformer equivalent circuit," *Automation of Electric Power Systems*, vol. 34, no. 9, pp. 72-76, May 2010. (in Chinese)

[36] A. G. Phadke and J. S. Thorp, *Computer Relaying for Power Systems*, 2nd ed., New York, USA: Wiley, 2009.

[37] Q. Yang and S. Huang, *Fundamentals of Microcomputer Relay Protection*, 2nd ed, Beijing, China: China Electric Power Press, 2005.

[38] C. M. Arturi, "Model of a highly saturated three-phase autotransformer with tertiary winding and five-limb core and analysis of a time-varying short-circuit transient," *European Transactions on Electrical Power*, vol. 4, no. 6, pp. 513-524, Dec. 1994.

[39] A. M. Shah, B. R. Bhalja, and R. M. Patel *et al.*, "Quartile based differential protection of power transformer," *IEEE Transactions on Power Delivery*, vol. 35, no. 5, pp. 2447-2458, Oct. 2020.

[40] M. Tripathy, R. P. Maheshwari, and H. K. Verma, "Power transformer differential protection based on optimal probabilistic neural network," *IEEE Transactions on Power Delivery*, vol. 25, no. 1, pp. 102-112, Jan. 2010.

[41] L. Zhuang. "A topology-based model for two-winding, shell-type, single-phase transformer inter-turn faults," M.S. thesis, University of Idaho, Moskow, USA, 2014.

[42] H. Wang and K. L. Butler, "Modeling transformers with internal incipient faults," *IEEE Transactions on Power Delivery*, vol. 17, no. 2, pp. 500-509, Feb. 2002.

[43] Manitoba Hydro International Ltd., "Custom-made duality-based transformer models for PSCAD," [Online]. Available: https://www.pscad.com/knowledge-base/article/597

[44] Z. Emin, M. Martinez-Duró, and M. V. Escudero *et al.*, "Transformer energization in power systems: a study guide," Cigre WG C4.307, Paris, France, Feb. 2014.